HHS Public Access

Author manuscript

Structure. Author manuscript; available in PMC 2024 May 04.

Published in final edited form as:

Structure. 2023 May 04; 31(5): 511–517.e3. doi:10.1016/j.str.2023.03.004.

Molecular insight into the PCNA-binding mode of FBH1

Jiuyang Liu[1,4], **Belén Chaves-Arquero**[2,4], **Pengcheng Wei**[3], **Adam H. Tencer**[1], **Antonio Ruiz-Albor**[2], **Gongyi Zhang**[3], **Francisco J. Blanco**[2,*], **Tatiana G. Kutateladze**[1,5,*]

[1]Department of Pharmacology, University of Colorado School of Medicine, Aurora, CO 80045, USA

[2]Centro de Investigaciones Biológicas Margarita Salas (CIB), CSIC, Madrid, 28040, Spain

[3]Department of Biomedical Research, National Jewish Health, Denver, CO 80206, USA

[4]Equal contribution

[5]Lead Contact

Summary

F-box DNA helicase 1 (FBH1) is involved in the regulation of cell responses to replicative stress. FBH1 is recruited to stalled DNA replication fork by PCNA where it inhibits homologous recombination and catalyzes fork regression. Here, we report the structural basis for the molecular recognition of two distinctly different motifs of FBH1, $FBH1_{PIP}$ and $FBH1_{APIM}$, by PCNA. The crystal structure of PCNA in complex with $FBH1_{PIP}$ and analysis of NMR resonance perturbations reveal overlapped $FBH1_{PIP}$ and $FBH1_{APIM}$ binding sites of PCNA and the dominant contribution of $FBH1_{PIP}$ in this interaction.

eTOC Blurb

Human enzyme FBH1 plays a major role in maintenance of the genome integrity. Liu et al. report the structural mechanism by which FBH1 is recruited to the DNA damaged sites.

Graphical Abstract

*Correspondence: fj.blanco@cib.csic.es or tatiana.kutateladze@cuanschutz.edu.

Authors contributions

J.L., B.C-A., P.W., T.A.H. and A.R-A. performed experiments and together with G.Z., F.J.B. and T.G.K. analyzed the data and prepared figures. J.L., F.J.B. and T.G.K. wrote the manuscript with input from all authors.

Declaration of interest

The authors declare no competing interests.

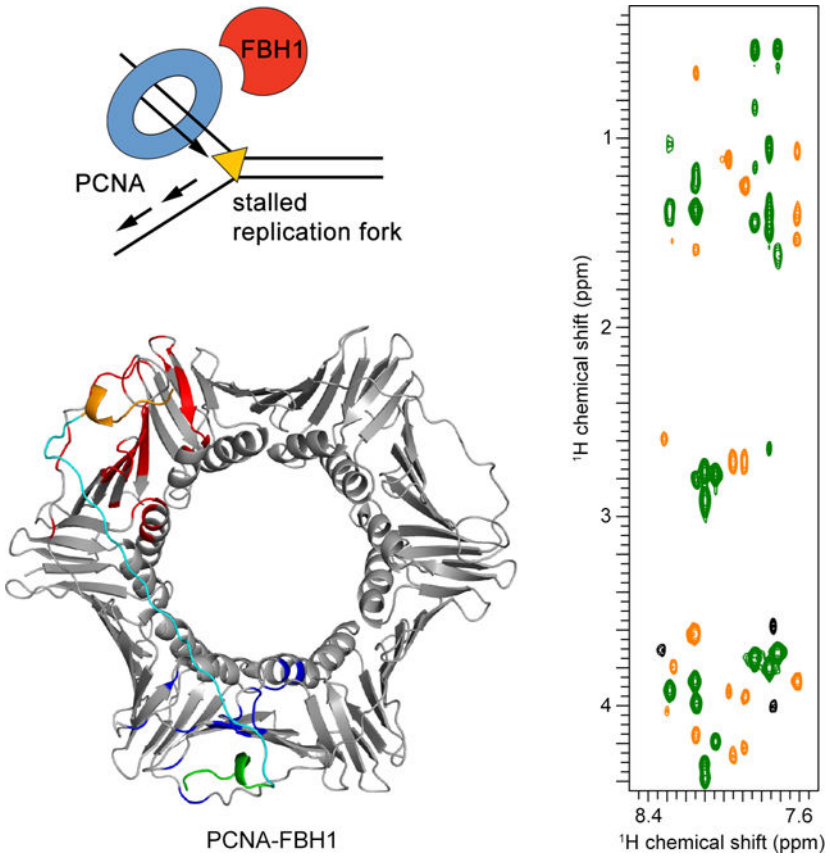

Keywords

PCNA; FBH1; PIP; APIM; mechanism

Introduction

F-box DNA helicase 1 (FBH1) plays a major role in maintenance of the genome integrity and stability.[1,2] It mediates the response to stalled or damaged DNA replication forks by impeding homologous recombination (HR). The anti-recombinogenic helicase activity of FBH1 was shown to be essential for repairing and restarting the replication fork.[3,4] FBH1 is recruited to the DNA damaged sites by proliferating cell nuclear antigen (PCNA) (Fig. 1a) and afterwards is polyubiquitinated and degraded through the Cullin-ring ligase 4-Cdt2 (CRL4Cdt2)–PCNA pathway.[5] It has been proposed that FBH1 polyubiquitination occurs simultaneously with PCNA monoubiquitination, which facilitates the recruitment of translesion DNA synthesis polymerase η to the DNA damaged site. In response to the DNA replication stalling arising from oncogenic stress, FBH1 promotes DNA double strand breaks and induces cellular apoptosis.[6,7] FBH1 deletion is frequently observed in melanoma, and defects in FBH1 are associated with the resistance of cancer cells to pharmacological treatment.[8] FBH1 also catalyzes the regression of stalled replication forks, triggering the response mediated by stress-activated protein kinases.[1] FBH1 is predicted to have two folded domains: a small F-box and a large catalytic ATP-binding UvrD-like

helicase domain,[9] and additionally two short motifs important for binding to PCNA were identified near the N- and C-terminal regions of the protein.[5]

PCNA is a key component of the chromatin remodeling and DNA replication and repair machineries in eukaryotic cells.[10] This large homotrimeric protein encircles DNA and tethers DNA polymerase complexes required for DNA synthesis, flap cleavage, and ligation to the replication fork.[11–13] PCNA is also a critical DNA damage response (DDR) factor that recruits DDR proteins to the DNA damaged sites to complete repair.[14,15] PCNA has a large number of binding partners, the majority of which contains a conserved PCNA-interacting protein (PIP) motif, characterized by the sequence Qxx*h*xx*aa*, where *h* is a hydrophobic aliphatic residue, *a* is an aromatic residue, and x is any residue.[16,17] Along with the canonical PIP motif ($FBH1_{PIP}$) near its N-terminus, FBH1 contains a second short motif within the C-terminal helicase domain. The AlkB homolog 2 PCNA-interacting motif ($FBH1_{APIM}$) is defined by the +*ah*x+ sequence, where + is a positively charged residue, *a* is an aromatic residue, *h* is a hydrophobic aliphatic residue, and x is any residue. It has been shown that both $FBH1_{PIP}$ and $FBH1_{APIM}$ motifs associate with PCNA, contributing to the accumulation of FBH1 at the stalled replication fork after DNA damage,[5] however the mechanistic basis underlying this association remains unclear.

Here, we describe the molecular mechanism by which FBH1 binds to PCNA via its $FBH1_{PIP}$ and $FBH1_{APIM}$ motifs. The crystal structure of the PCNA-$FBH1_{PIP}$ complex and analysis of NMR resonance perturbations in PCNA suggest overlapped binding sites for $FBH1_{PIP}$ and $FBH1_{APIM}$ and tighter binding of $FBH1_{PIP}$.

Results and discussion

To determine the structural basis for the interaction between PCNA and FBH1, we produced isotopically enriched PCNA and recorded its $^{1}H,^{15}N$ TROSY spectra before and after the addition of increasing amounts of $FBH1_{PIP}$ (residues 55–68 of FBH1) peptide at 35 °C (Fig. 1b, c). We observed large chemical shift perturbations (CSPs) in backbone amides of PCNA, characterized by shifting and broadening of the resonances, indicating tight interaction in the intermediate exchange regime on the chemical shift timescale. In agreement, fitting analysis of CSPs for 10 PCNA signals yielded a dissociation constant (K_d) of 7.8 ± 3.7 μM (Fig. 1b, d). The perturbed PCNA regions include residues M40-Q49, L121-Y133 and M199-E258 (Fig. 1e). In addition to the amide resonances that exhibited changes larger than the mean plus two standard deviations, several perturbed signals broadened beyond detection upon peptide binding (indicated by red ovals in Fig. 1e). CSP analysis suggests that these perturbed residues comprise the $FBH1_{PIP}$-binding pocket of PCNA.

To gain insight into the binding mechanism, we co-crystallized PCNA with $FBH1_{PIP}$ and determined the crystal structure of the PCNA-$FBH1_{PIP}$ complex, refining the structure to a 1.9 Å resolution (Table 1). In the complex, three molecules/protomers of PCNA self-assemble into a ring-shaped structure (Fig. 2a), which is very similar to the structure of free PCNA (RMSD = 0.5 Å for the Cα atoms). Each protomer is bound to one $FBH1_{PIP}$ peptide (Fig. 2a, b). The electron-density map of $FBH1_{PIP}$ from Q57 to F64 can be unambiguously traced in the electron density map of three molecules, S56 only in one of them, and

residues G55 and L65-K68 were not observed (Fig. 2c). The $FBH1_{PIP}$ peptide occupies a hydrophobic groove formed by several loops of PCNA, including the long interdomain connector loop (IDCL), and the C-terminal end of PCNA. The $FBH1_{PIP}$ region from I60 to F63 adopts a 3_{10}-helix structure, which is stabilized by intramolecular hydrogen bonds between the carbonyl group of I60 and the backbone amides of F63 and F64, and between the carbonyl group of C59 and the backbone amide of E62. The carboxyl group of E62 in the bound state of $FBH1_{PIP}$ is engaged in water-mediated hydrogen bonds with the backbone amide of C59.

A network of intermolecular hydrogen bonds and hydrophobic contacts stabilize the complex. The key signature residue of the PIP motif, Q57 is bound in the so-called Q-pocket of PCNA (Fig. 2d). The sidechain amide group of Q57 is the donor in a hydrogen bond with the backbone carbonyl group of A252 of PCNA, whereas the sidechain carbonyl group of Q57 is restrained through water-mediated hydrogen bonds with the amino group of K254 and the backbone amide of A208 of PCNA (Fig. 2e). Notably, a similar mode for recognition of Q in PIP sequences is frequently observed in other PCNA-PIP complexes.[18] The PCNA-$FBH1_{PIP}$ complex is further stabilized by the backbone-backbone hydrogen bonds involving the amides of R58 and I60 of $FBH1_{PIP}$ and the carbonyls of P253 and H44 of PCNA. The side chains of I60 and F64 in $FBH1_{PIP}$ are buried in a deep hydrophobic pocket lined by PCNA residues L47, L126, I128, P129, P234, Y250 and A252. Particularly, the benzene ring of F64 inserts into a cavity formed by P129, P234 and Y250. We note that the $FBH1_{PIP}$-binding site residues of PCNA were perturbed in NMR titration experiments (Fig. 1e). Mapping the most perturbed residues onto the structure of the PCNA-$FBH1_{PIP}$ complex delineated the $FBH1_{PIP}$-binding pocket (Fig. 2f). Substantial overlap of this CSPs-derived binding site and the binding site seen in the crystal structure of the complex indicated that the $FBH1_{PIP}$ binding mode is the same in the crystal and in solution.

The noteworthy feature of FBH1 that distinguishes this protein from other binding partners of PCNA is the presence of two dissimilar PCNA binding motives, the Qxx*h*xx*aa* sequence in the N-terminal region of the protein and the +*ah*x+ sequence in the C-terminal region (Fig. 3a). The structure of FBH1 predicted by AlphaFold suggests that $FBH1_{PIP}$ is located in a disordered region of FBH1, whereas $FBH1_{APIM}$ is located in the folded UvrD helicase domain (Fig. 3b). To understand how PCNA recognizes the two dissimilar FBH1 sequences, we characterized the interaction of PCNA with a $FBH1_{APIM}$ by NMR titration experiments (Fig. 3c–g). Unlabeled $FBH1_{APIM}$ (residues 805–815 of FBH1) peptide was added into labeled PCNA and following each addition NMR spectra were collected (Fig. 3c). Large perturbations were observed for a set of PCNA signals, and some of these signals were also perturbed (primarily disappeared) upon addition of the $FBH1_{PIP}$ peptide (Figs. 1e and 3g). We note that upon titration with $FBH1_{APIM}$, the PCNA amide resonances shifted rather than broadened (Fig. 3d), indicating fast exchange regime on the NMR time scale and a reduced affinity compared to the affinity of PCNA to $FBH1_{PIP}$. Indeed, a K_d of 276 ± 84 μM was measured using 15 PCNA signals that exhibited changes larger than the mean plus two standard deviations (Fig. 3e). Mapping CSPs on the structure of PCNA shows that the $FBH1_{APIM}$ peptide binds to the same region of PCNA as $FBH1_{PIP}$ (Fig. 3f). The patterns of

CSPs caused by the two peptides were not identical but their similarity indicates an overlap of the binding sites.

Co-immunoprecipitation assays following local ultraviolet irradiation suggest that PCNA recruits FBH1 to the DNA damaged sites, and a reduced co-localization of PCNA and FBH1 when either PIP or APIM is mutated indicates that both motifs contribute to the interaction with PCNA at the replication fork.[5] The centers of two adjacent binding sites on the same side of the PCNA ring are approximately 60 Å apart (Fig. 2a). This separation is within the range of distances between the two motifs in the AlphaFold predicted model of FBH1 (Fig. 3b), which would allow both motifs to simultaneously bind to one PCNA trimer. Docking $FBH1_{PIP}$ and $FBH1_{APIM}$ to adjacent protomers of the PCNA ring using CSPs as restraints in HADDOCK supported the capability of FBH1 to engage both motifs concurrently (Fig. 4a). Modeling also revealed that a 25-glycine linker (~70 Å) is sufficient to connect $FBH1_{PIP}$ and $FBH1_{APIM}$ in the complex (Fig. 4a). Binding of $FBH1_{PIP}$ and $FBH1_{APIM}$ to the same sites of the PCNA protomers was confirmed by ^{1}H-^{1}H TOCSY competitive binding experiments (Fig. 4b, c). An increase in the intensity of the signals of free $FBH1_{PIP}$ upon titration with $FBH1_{APIM}$ indicated that $FBH1_{PIP}$ is displaced from the complex (Fig. 4c, d).

Despite $FBH1_{PIP}$ binds tighter than $FBH1_{APIM}$, the dual interaction can increase macroscopic affinity due to the avidity effect and increased apparent local concentration of the motifs. The ability of FBH1 to dimerize[3] can further enhance this interaction. However, according to the AlphaFold generated structure of the FBH1 UvrD helicase, $FBH1_{APIM}$ forms an amphipathic α-helix in which the hydrophobic side, likely involved in the interaction with PCNA, is partially buried in the core of the helicase domain and therefore is not readily accessible for the interaction with PCNA (Fig. 4e). The UvrD helicases have been shown to undergo large-scale conformational changes upon binding to DNA.[19] Overlay of the UvrD domain from FBH1 and the crystal structure of the *Deinococcus radiodurans* UvrD in complex with DNA[19] suggests a proximity of the $FBH1_{APIM}$ helix to DNA (Fig. 4f). The interaction of the positively charged side of the $FBH1_{APIM}$ amphipathic α-helix with DNA could provide a mechanism by which the hydrophobic side of the helix can be released for the association with PCNA or other binding partners.

$FBH1_{PIP}$ and $FBH1_{APIM}$ motifs have been shown to be essential in FBH1 functions *in vivo*,[5] and mutations in both are found in cancer patients (Cosmic, cBioPortal). Particularly, Q57E mutation in $FBH1_{PIP}$ and I860M (corresponds to I809 in isoform 1) in $FBH1_{APIM}$, which are associated with cervical squamous cell carcinoma and breast cancer, suggest that the PCNA-FBH1 signaling pathway may play a role in the pathophysiology of these diseases. Future studies are required to better understand the physiological importance of this signaling pathway, establish the mechanism by which PCNA and FBH1 form a complex at the DNA damaged sites and explore the implication of FBH1 polyubiquitination.

STAR METHODS

RESOURCE AVAILABILITY

Lead contact—Further information and requests for resources and reagents should be directed to and will be fulfilled by the lead contact, Tatiana G. Kutateladze (tatiana.kutateladze@cuanschutz.edu).

Materials availability—All expression plasmids used in this study will be made available on request. This study did not generate new unique reagents.

Data and code availability—Coordinates and structure factors have been deposited in the Protein Data Bank under the accession code 8F5Q. Other data reported in this paper will be shared by the lead contact upon request. This paper does not report original code. Any additional information required to reanalyze the data reported in this paper is available from the lead contact upon request.

EXPERIMENTAL MODEL AND SUBJECT DETAILS

PCNA was expressed in BL21 (DE3) RIL in Luria Broth or isotopically enriched media. Protein production was induced with 0.5 mM IPTG for 18 h at 16°C.

METHOD DETAILS

Protein expression and purification—The cDNA of full length human PCNA was cloned into a pET-47b vector. The protein was expressed in *Escherichia coli* BL21 (DE3) RIL cells grown in Luria Broth and induced with 0.5 mM IPTG for 18 h at 16 °C. Bacteria were harvested by centrifugation and lysed by sonication. His-tagged PCNA was purified on HisPur Ni-NTA agarose beads (Thermo-Fisher) in 20 mM Tris-HCl pH 7.5, 500 mM NaCl and 2 mM DTT buffer. The His-tag was cleaved overnight at 4 °C with PreScission protease. The untagged protein was further purified by size exclusion chromatography on a HiPrep 16/60 Sephacryl S200 HR column in 20 mM Tris-HCl pH 7.5, 150 mM NaCl and 2 mM DTT buffer. The unlabeled PCNA was used in crystallization. For NMR experiments, uniformly $^{2}H,^{13}C,^{15}N$-PCNA was prepared as described.[20]

NMR spectroscopy—^{1}H-^{15}N BEST-TROSY spectra were acquired on a Bruker AVANCE NEO 800 MHz spectrometer equipped with a TCI cryo-probe and z-gradients at 35 °C for 23 h. The samples contained 400 μl of 50 μM U-[$^{2}H,^{13}C,^{15}N$] PCNA in PBS (10 mM phosphate, 140 mM chloride, 153 mM sodium, and 4.5 mM potassium) pH 7.0 buffer, supplemented with 20 μM DSS (4,4-dimethyl-4-silapentane-1-sulfonic acid), 0.01 % NaN3, 1 mM DTT and 5 % $^{2}H_{2}O$. The binding was characterized by monitoring CSPs in the ^{1}H-^{15}N TROSY spectra of PCNA as $FBH1_{PIP}$ (^{55}GSQRCIPEFFLAGK^{68}) or $FBH1_{APIM}$ (^{805}KDKFIRRWVHK^{815}) peptides were added stepwise.

The dissociation constants were determined with GraphPad Prism 9.1 by a nonlinear least-squares regression using the equation:

$$CSP = \left(K_d + [P] + R[P] - \sqrt{\left(K_d + [P] + R[P]^2 - \left(4R[P]^2\right)\right)}\right)/2[P]CSP_{max}$$

where CSP is the weighted average of the ^{1}H and ^{15}N chemical shift perturbations measured at each titration point, K_d is the dissociation constant assuming a 1:1 stoichiometry, [P] is the concentration of PCNA protomer at the first point of the titration, R is the [peptide]/[PCNA protomer] ratio at each point of the titration, and CSP_{max} is the CSP at saturation. Weighted average CSP values[21] were calculated using the equation

$$CSP = \sqrt{\left(\left(\Delta\delta^{1}H\right)^2 + \left(\Delta\delta^{15}N/5\right)^2\right)/2}$$

where Δδ is the change in chemical shift in parts per million (ppm). The K_d values represent the average measured for 10–15 PCNA backbone amides, and the errors represent the average of the standard errors. NMR data were processed using TopSpin v4.1 (Bruker) and analyzed using CcpNmr Analysis v2.[22]

^{1}H-^{1}H TOCSY NMR spectra were acquired on a 600 MHz Bruker Avance NMR spectrometer at 5 °C for 1.5 h. All protein samples were in PBS pH 7.0 buffer, supplemented with 25 μM DSS and 5 % $^{2}H_2O$. ^{1}H-^{1}H TOCSY spectra were collected on 25 μM PCNA, while first $FBH1_{PIP}$ and then $FBH1_{APIM}$ were added. Signal intensities (cross-peak height) from unbound $FBH1_{PIP}$ were scaled to compensate for sample dilution. Reference ^{1}H-^{1}H TOCSY spectra were acquired on 50 μM $FBH1_{PIP}$ and 50 μM of $FBH1_{APIM}$.

Crystallization, data collection, and structure determination—PCNA (5 mg/mL) was incubated with the $FBH1_{PIP}$ peptide (residues 55–68, in a 1:3 protein-to-peptide molar ratio) at room temperature for 20 min. Crystals were obtained at room temperature using the sitting-drop vapor diffusion method by mixing equal volumes of protein solution with well solution composed of 0.1 M HEPES pH 7.5, 0.2 M $MgCl_2$, 30% PEG 400. X-ray diffraction data were collected from a single crystal at the ALS 4.2.2 beamline, Berkeley, administrated by the Molecular Biology Consortium. The diffraction data were processed using the iMosflm program 6[23], then scaled by Aimless Pointless in the CCP4 software suite 7[24]. The structure was determined by molecular replacement using the program PHASER,[25] the monomer of PCNA structure (PDB code: 5IY4) [26] was used as a search model. The models from the molecular replacement were built using Crystallographic Object-Oriented Toolkit program 9[27] and subsequently subjected to refinement using PHENIX software.[28] Crystallography diffraction data collection and refinement statistics are summarized in Table 1.

HADDOCK docking—High Ambiguity Driven Biomolecular DOCKing (HADDOCK) runs were performed using the interface of the WeNMR/West-Life GRID-enabled web portal for HADDOCK.2.4 and standard parameters[29] on the crystal structures of free PCNA (PDB ID: 1VYM) and $FBH1_{PIP}$-bound PCNA. $FBH1_{APIM}$ (KJKFIRRW sequence) was homology modeled using the crystal structure of APIM from the ZRANB3 protein bound to PCNA (PDB ID: 5ID8). For $FBH1_{PIP}$ docking to one PCNA protomer, the PCNA residues

whose NMR signals exhibited changes larger than average plus two standard deviations or disappeared were marked as active, whereas the passive residues were determined automatically. The structure with the best HADDOCK score was selected for docking the $FBH1_{APIM}$ sequence to a different protomer (active residues were identified from Fig. 3g). The structure with the best score was selected to connect the C-terminal residue of $FBH1_{PIP}$ with the N-terminal residue of $FBH1_{APIM}$ through a polyglycine linker of variable length modeled manually with the building and sculpting tools of PyMol (http://www.pymol.org/pymol). The quality of the model was evaluated by MolProbity.[30] The MolProbity clash score was found to be similar for PCNA with the docked peptides without or with a 25-residue polyglycine linker (12.97 and 11.84, respectively).

QUANTIFICATION AND STATISTICAL ANALYSIS

The crystal structure of PCNA in complex with three $FBH1_{PIP}$ was determined using materials and softwares listed in the Key Resources Table and method section. Statistics generated from X-ray crystallography data processing, refinement, and structure validation are displayed in Table 1. The K_d values for the interaction of PCNA with $FBH1_{PIP}$ and $FBH1_{APIM}$ were measured by NMR and represent weighted average ± SD for 15 PCNA signals and 10 PCNA signals, respectively. NMR experiments were performed once using materials and softwares listed in the Key Resources Table and method section.

Acknowledgments

This work was supported in part by NIH grants HL151334, CA252707, GM125195, GM135671 and AG067664 to T.G.K., Spanish Ministry of Science and Education grant PID2020-113225GB-I00 to F.J.B. and the predoctoral contract PRE2021-099992 to A.R.A. Some of the NMR spectra were recorded at the ICTS facility of the CSIC Laboratorio de RMN Manuel Rico.

REFERENCES

1. Fugger K, Mistrik M, Neelsen KJ, Yao Q, Zellweger R, Kousholt AN, Haahr P, Chu WK, Bartek J, Lopes M, et al. (2015). FBH1 Catalyzes Regression of Stalled Replication Forks. Cell reports 10, 1749–1757. 10.1016/j.celrep.2015.02.028. [PubMed: 25772361]
2. Sakaguchi C, Morishita T, Shinagawa H, and Hishida T. (2008). Essential and distinct roles of the F-box and helicase domains of Fbh1 in DNA damage repair. BMC molecular biology 9, 27. 10.1186/1471-2199-9-27. [PubMed: 18312697]
3. Fugger K, Mistrik M, Danielsen JR, Dinant C, Falck J, Bartek J, Lukas J, and Mailand N. (2009). Human Fbh1 helicase contributes to genome maintenance via pro- and anti-recombinase activities. The Journal of cell biology 186, 655–663. 10.1083/jcb.200812138. [PubMed: 19736316]
4. Chiolo I, Saponaro M, Baryshnikova A, Kim JH, Seo YS, and Liberi G. (2007). The human F-Box DNA helicase FBH1 faces Saccharomyces cerevisiae Srs2 and postreplication repair pathway roles. Molecular and cellular biology 27, 7439–7450. 10.1128/MCB.00963-07. [PubMed: 17724085]
5. Bacquin A, Pouvelle C, Siaud N, Perderiset M, Salomé-Desnoulez S, Tellier-Lebegue C, Lopez B, Charbonnier JB, and Kannouche PL (2013). The helicase FBH1 is tightly regulated by PCNA via CRL4(Cdt2)-mediated proteolysis in human cells. Nucleic acids research 41, 6501–6513. 10.1093/nar/gkt397. [PubMed: 23677613]
6. Fugger K, Chu WK, Haahr P, Kousholt AN, Beck H, Payne MJ, Hanada K, Hickson ID, and Sorensen CS (2013). FBH1 co-operates with MUS81 in inducing DNA double-strand breaks and cell death following replication stress. Nature communications 4, 1423. 10.1038/ncomms2395.
7. Jeong YT, Rossi M, Cermak L, Saraf A, Florens L, Washburn MP, Sung P, Schildkraut CL, and Pagano M. (2013). FBH1 promotes DNA double-strand breakage and apoptosis in response to DNA

replication stress. The Journal of cell biology 200, 141–149. 10.1083/jcb.201209002. [PubMed: 23319600]

8. Jeong YT, Cermak L, Guijarro MV, Hernando E, and Pagano M. (2013). FBH1 protects melanocytes from transformation and is deregulated in melanomas. Cell cycle 12, 1128–1132. 10.4161/cc.24165. [PubMed: 23466708]
9. Kim J, Kim J-H, Lee S-H, Kim D-H, Kang H-Y, Bae S-H, Pan Z-Q, and Seo Y-S (2002). The Novel Human DNA Helicase hFBH1 Is an F-box Protein *. Journal of Biological Chemistry 277, 24530–24537. 10.1074/jbc.M201612200. [PubMed: 11956208]
10. Moldovan GL, Pfander B, and Jentsch S. (2007). PCNA, the maestro of the replication fork. Cell 129, 665–679. 10.1016/j.cell.2007.05.003. [PubMed: 17512402]
11. Kelman Z. (1997). PCNA: structure, functions and interactions. Oncogene 14, 629–640. 10.1038/sj.onc.1200886. [PubMed: 9038370]
12. Matsumoto Y, Brooks RC, Sverzhinsky A, Pascal JM, and Tomkinson AE (2020). Dynamic DNA-bound PCNA complexes co-ordinate Okazaki fragment synthesis, processing and ligation. Journal of molecular biology 432, 166698. 10.1016/j.jmb.2020.10.032.
13. González-Magaña A, and Blanco FJ (2020). Human PCNA Structure, Function and Interactions. Biomolecules 10. 10.3390/biom10040570.
14. Cazzalini O, Sommatis S, Tillhon M, Dutto I, Bachi A, Rapp A, Nardo T, Scovassi AI, Necchi D, Cardoso MC, et al. (2014). CBP and p300 acetylate PCNA to link its degradation with nucleotide excision repair synthesis. Nucleic acids research 42, 8433–8448. 10.1093/nar/gku533. [PubMed: 24939902]
15. Essers J, Theil AF, Baldeyron C, van Cappellen WA, Houtsmuller AB, Kanaar R, and Vermeulen W. (2005). Nuclear dynamics of PCNA in DNA replication and repair. Molecular and cellular biology 25, 9350–9359. 10.1128/MCB.25.21.9350-9359.2005. [PubMed: 16227586]
16. Warbrick E. (2000). The puzzle of PCNA's many partners. BioEssays : news and reviews in molecular, cellular and developmental biology 22, 997–1006. 10.1002/1521-1878(200011)22:11<997::aid-bies6>3.0.co;2-#.
17. De Biasio A, and Blanco FJ (2013). Proliferating cell nuclear antigen structure and interactions: too many partners for one dancer? Advances in protein chemistry and structural biology 91, 1–36. 10.1016/B978-0-12-411637-5.00001-9. [PubMed: 23790209]
18. Gulbis JM, Kelman Z, Hurwitz J, O'Donnell M, and Kuriyan J. (1996). Structure of the C-terminal region of p21(WAF1/CIP1) complexed with human PCNA. Cell 87, 297–306. 10.1016/s0092-8674(00)81347-1. [PubMed: 8861913]
19. Stelter M, Acajjaoui S, McSweeney S, and Timmins J. (2013). Structural and mechanistic insight into DNA unwinding by Deinococcus radiodurans UvrD. PloS one 8, e77364. 10.1371/journal.pone.0077364. [PubMed: 24143224]
20. Sanchez R, Torres D, Prieto J, Blanco FJ, and Campos-Olivas R. (2007). Backbone assignment of human proliferating cell nuclear antigen. Biomolecular NMR assignments 1, 245–247. 10.1007/s12104-007-9068-2. [PubMed: 19636876]
21. De Biasio A, Campos-Olivas R, Sanchez R, Lopez-Alonso JP, Pantoja-Uceda D, Merino N, Villate M, Martin-Garcia JM, Castillo F, Luque I, and Blanco FJ (2012). Proliferating cell nuclear antigen (PCNA) interactions in solution studied by NMR. PloS one 7, e48390. 10.1371/journal.pone.0048390.
22. Vranken WF, Boucher W, Stevens TJ, Fogh RH, Pajon A, Llinas M, Ulrich EL, Markley JL, Ionides J, and Laue ED (2005). The CCPN data model for NMR spectroscopy: development of a software pipeline. Proteins 59, 687–696. [PubMed: 15815974]
23. Battye TG, Kontogiannis L, Johnson O, Powell HR, and Leslie AG (2011). iMOSFLM: a new graphical interface for diffraction-image processing with MOSFLM. Acta crystallographica. Section D, Biological crystallography 67, 271–281. 10.1107/S0907444910048675. [PubMed: 21460445]
24. Winn MD, Ballard CC, Cowtan KD, Dodson EJ, Emsley P, Evans PR, Keegan RM, Krissinel EB, Leslie AG, McCoy A, et al. (2011). Overview of the CCP4 suite and current developments. Acta crystallographica. Section D, Biological crystallography 67, 235–242. 10.1107/S0907444910045749. [PubMed: 21460441]

25. McCoy AJ, Grosse-Kunstleve RW, Adams PD, Winn MD, Storoni LC, and Read RJ (2007). Phaser crystallographic software. Journal of applied crystallography 40, 658–674. 10.1107/S0021889807021206. [PubMed: 19461840]

26. Wang Y, Xu M, and Jiang T. (2016). Crystal structure of human PCNA in complex with the PIP box of DVC1. Biochemical and Biophysical Research Communications 474, 264–270. 10.1016/j.bbrc.2016.04.053. [PubMed: 27084448]

27. Emsley P, and Cowtan K. (2004). Coot: model-building tools for molecular graphics. Acta crystallographica. Section D, Biological crystallography 60, 2126–2132. [PubMed: 15572765]

28. Adams PD, Grosse-Kunstleve RW, Hung LW, Ioerger TR, McCoy AJ, Moriarty NW, Read RJ, Sacchettini JC, Sauter NK, and Terwilliger TC (2002). PHENIX: building new software for automated crystallographic structure determination. Acta crystallographica. Section D, Biological crystallography 58, 1948–1954. [PubMed: 12393927]

29. Honorato RV, Koukos PI, Jimenez-Garcia B, Tsaregorodtsev A, Verlato M, Giachetti A, Rosato A, and Bonvin A. (2021). Structural Biology in the Clouds: The WeNMR-EOSC Ecosystem. Front Mol Biosci 8, 729513. 10.3389/fmolb.2021.729513.

30. Williams CJ, Headd JJ, Moriarty NW, Prisant MG, Videau LL, Deis LN, Verma V, Keedy DA, Hintze BJ, Chen VB, et al. (2018). MolProbity: More and better reference data for improved all-atom structure validation. Protein Sci 27, 293–315. 10.1002/pro.3330. [PubMed: 29067766]

Highlights

- Divergent PIP and APIM motifs of FBH1 bind PCNA
- The PIP and APIM binding sites of PCNA overlap
- PCNA shows greater affinity to the PIP motif

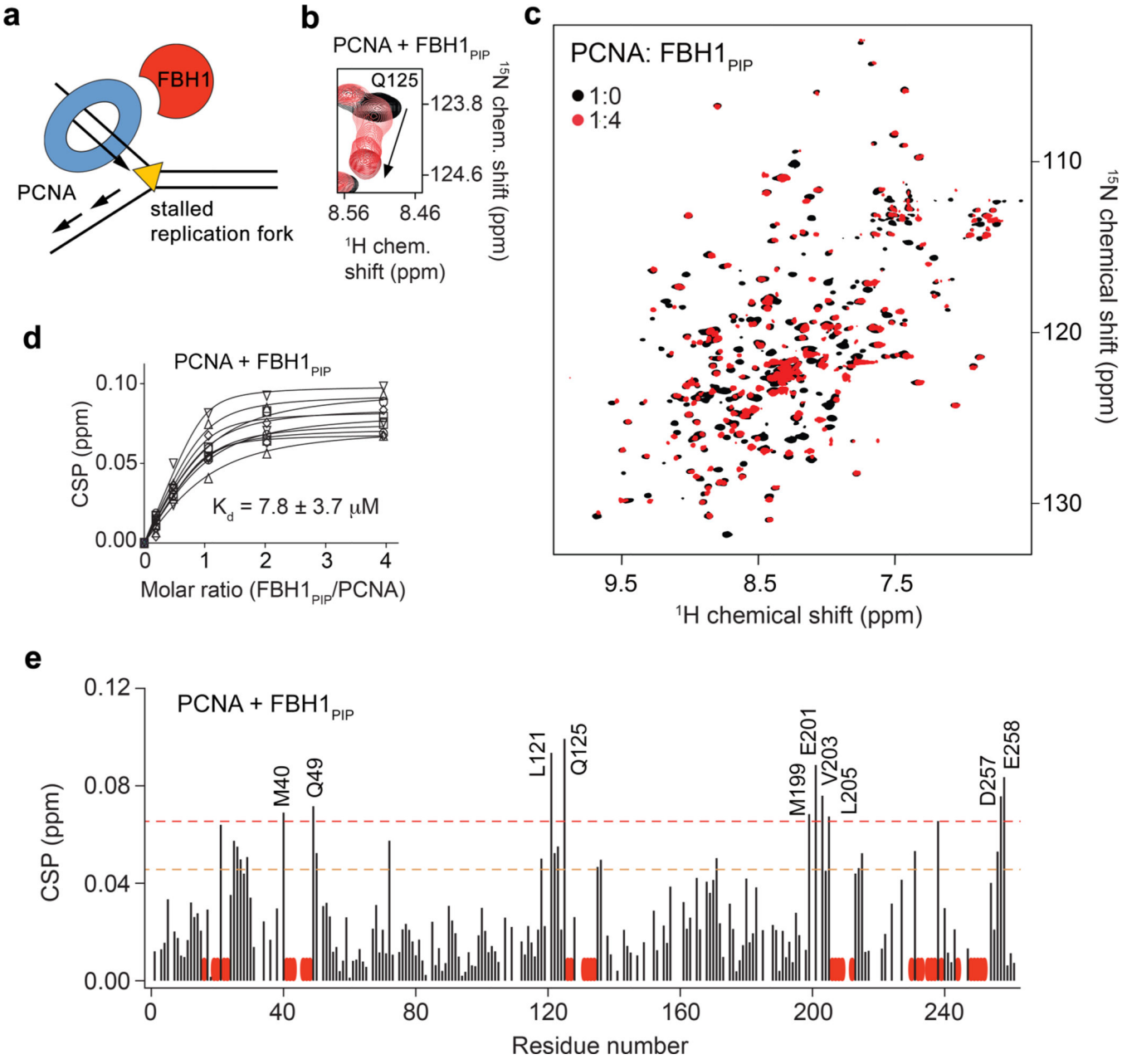

Figure 1. FBH1 binds to PCNA through the PIP motif.

(a) A schematic showing the recruitment of FBH1 to the damaged replication fork by PCNA. (b) Overlay of a selected region of $^{1}H,^{15}N$ TROSY spectra of isotopically enriched PCNA showing the backbone amide signal of Q125 (black) and its shift with increasing $FBH1_{PIP}$ peptide:PCNA molar ratios (1:0.2, 1:0.5, 1:1, 1:2, and 1:4, all in red). (c) Overlay of the full $^{1}H,^{15}N$ TROSY spectra of PCNA collected before (black) and after addition of 4-fold molar excess of $FBH1_{PIP}$ peptide (red). (d) Binding curves used to determine the K_d value for the interaction of $FBH1_{PIP}$ with PCNA by NMR. (e) Bar graph of normalized CSPs in the spectra of PCNA induced by 4-fold molar excess of $FBH1_{PIP}$ as a function

of residue. The dotted lines indicate the mean plus one (orange) or two (red) standard deviations. Red ovals indicate signals broadened beyond detection.

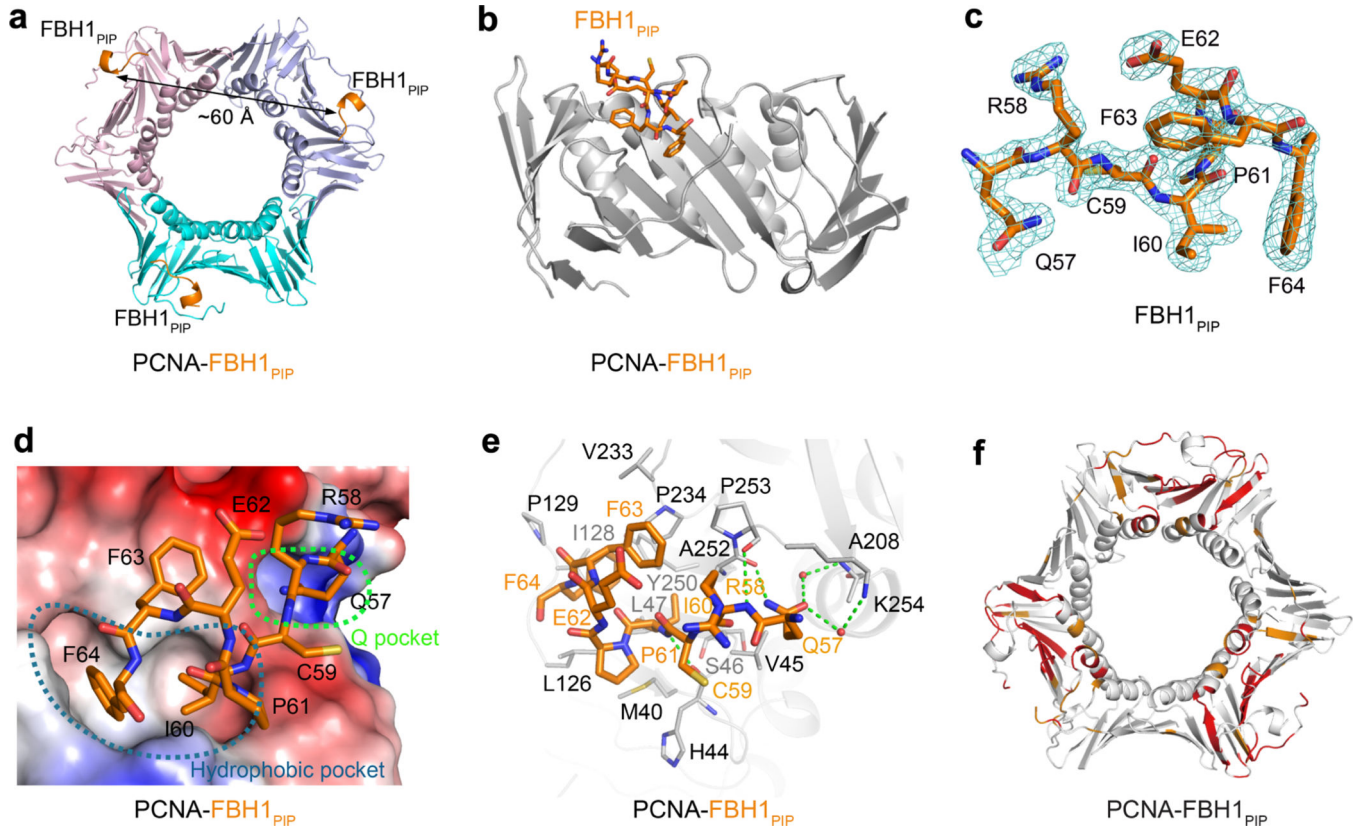

Figure 2. Structural basis of FBH1$_{PIP}$ binding to PCNA.

(a) Ribbon diagram of the crystal structure of trimeric PCNA in complex with three FBH1$_{PIP}$ molecules (orange). The three PCNA protomers are colored pink, blue and cyan. (b) Diagram of one PCNA protomer (grey ribbon) with bound FBH1$_{PIP}$ shown as orange sticks. (c) The $2F_o$-F_c electron-density map (cyan mesh) of FBH1$_{PIP}$ (orange sticks) contoured at 1 σ. (d) Electrostatic surface potential of PCNA colored blue and red for positive and negative charges, respectively, at the FBH1$_{PIP}$-binding site. The Q-pocket and the hydrophobic pockets are indicated, and the FBH1$_{PIP}$ molecule is displayed with sticks (e) A zoom-in-view of the FBH1$_{PIP}$-binding site of PCNA. PCNA residues are labeled in black and FBH1$_{PIP}$ residues are labeled in orange. Green dashed lines and red spheres indicate hydrogen bonds and water molecules, respectively. (f) PCNA residues that exhibit FBH1$_{PIP}$-induced resonance changes are mapped onto the crystal structure of PCNA-FBH1$_{PIP}$ and colored red (CSP larger than average plus two standard deviations or signal disappearance) or orange (CSP larger than average plus one standard deviation).

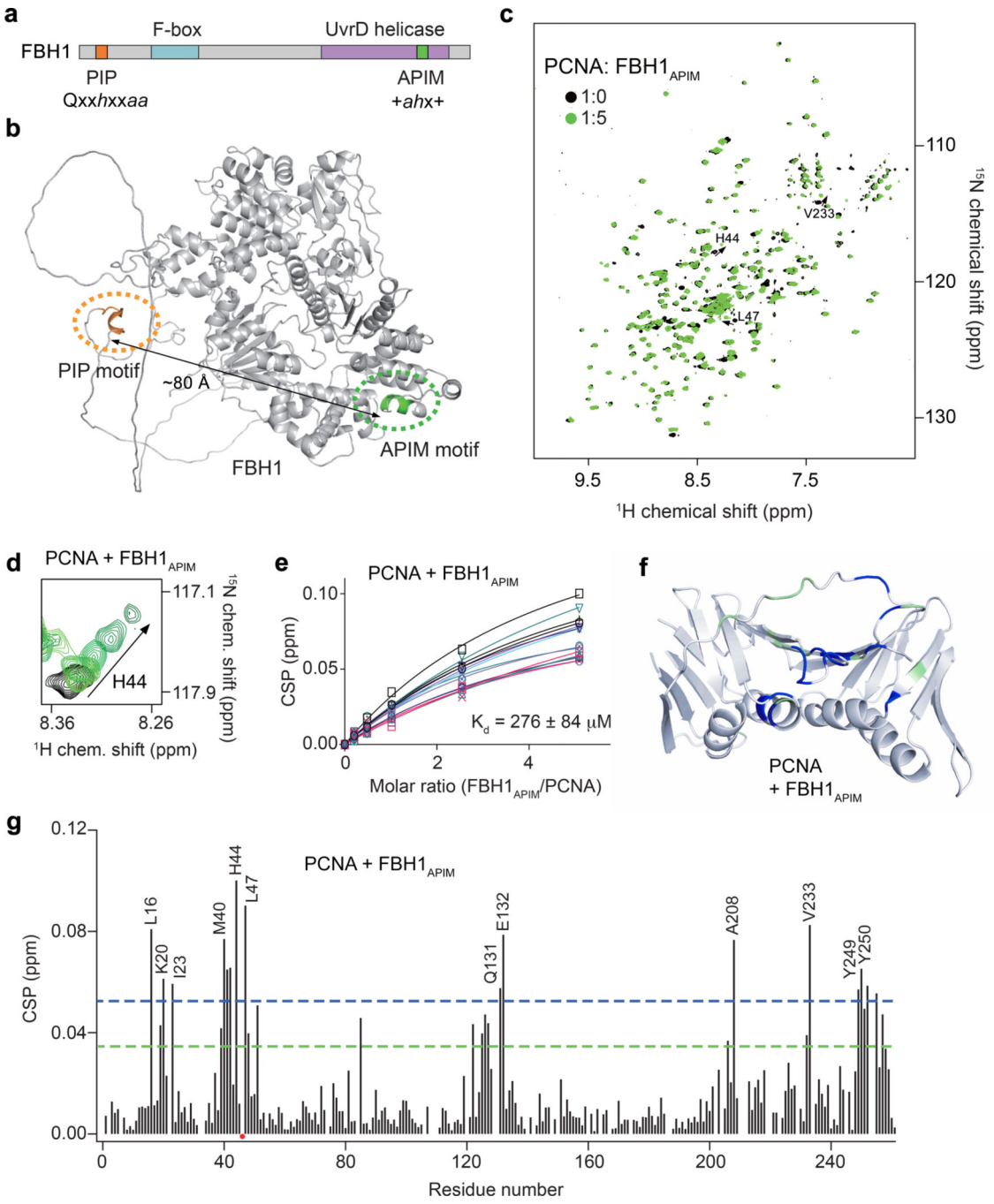

Figure 3. FBH1$_{APIM}$ and FBH1$_{PIP}$ binding sites of PCNA overlap.

(a) FBH1 domain architecture. The FBH1$_{PIP}$ and FBH1$_{APIM}$ motifs are highlighted in orange and green. (b) AlphaFold model of the human FBH1 structure from UniProt Q8NFZ0. FBH1$_{PIP}$ and FBH1$_{APIM}$ are indicated by dashed ovals. (c) Overlay of ^{1}H,^{15}N TROSY spectra of isotopically enriched PCNA collected before (black) and after addition of 5-fold molar excess of FBH1$_{APIM}$ peptide (green). (d) Overlay of a selected region of ^{1}H,^{15}N TROSY spectra of PCNA showing the backbone amide signal of H44 (black) and its shift with increasing FBH1$_{APIM}$ peptide:PCNA molar ratios (1:0.2, 1:0.5, 1:1, 1:2.5, and

1:5, all in green). (e) Binding curves used to determine the K_d value for the interaction of $FBH1_{APIM}$ with PCNA by NMR. (f) PCNA residues that exhibit CSP larger than the average plus one (green) or two (blue) standard deviations upon addition of 5-fold $FBH1_{APIM}$ are indicated on the crystal structure of one PCNA protomer. (g) Bar graph of CSPs in $^{1}H,^{15}N$ TROSY spectra of PCNA induced by 5-fold molar excess of $FBH1_{APIM}$ as a function of residue. The dotted lines indicate the mean plus one (green) and two (blue) standard deviations. The red dot indicates a very weak signal that disappears after the first peptide addition.

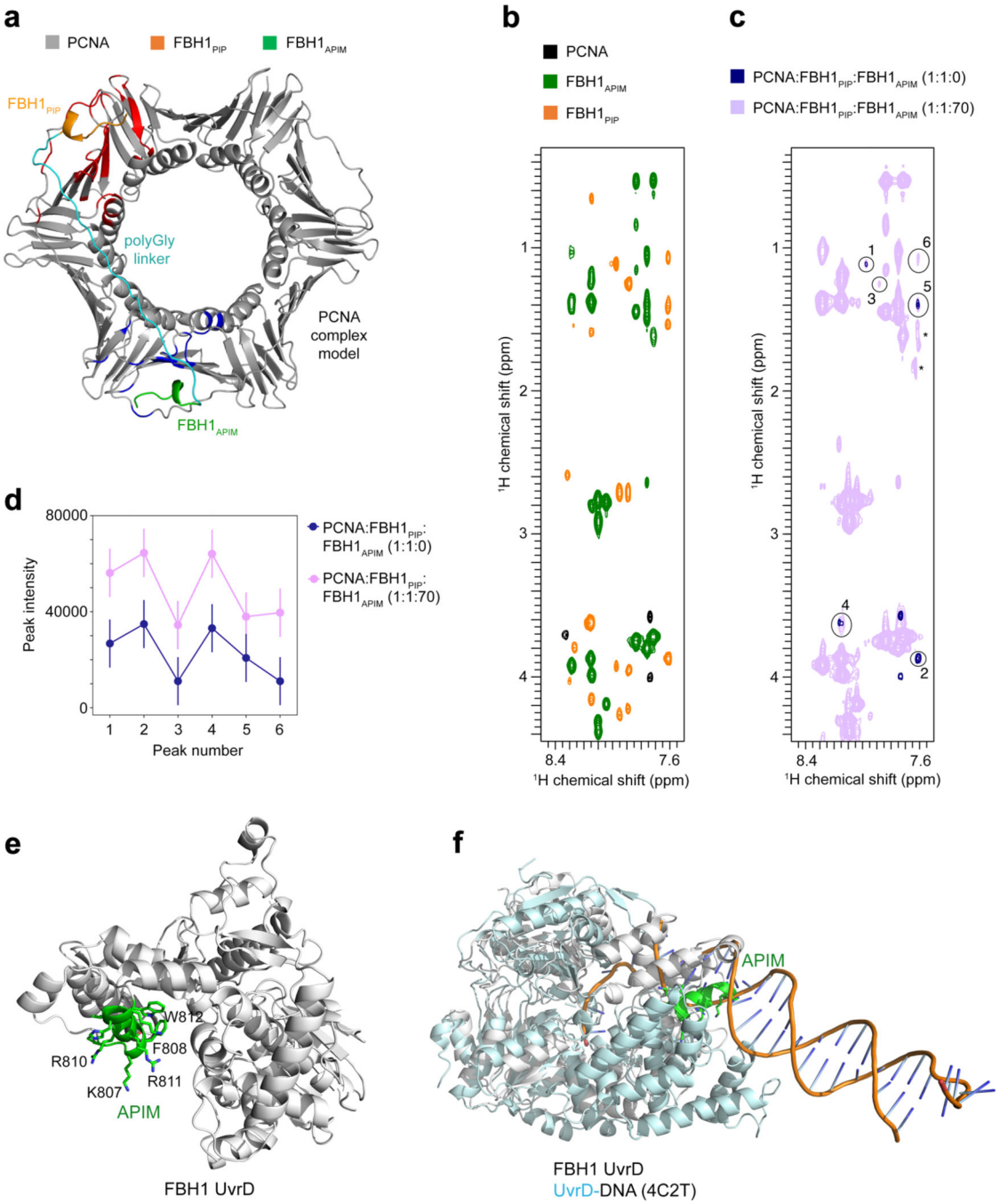

Figure 4. Bivalent binding and accessibility of FBH1$_{APIM}$.

(a) CSPs-guided HADDOCK model of the PCNA ring with docked FBH1$_{PIP}$ (orange) and FBH1$_{APIM}$ (green) connected by a 25-residue polyglycine linker (cyan). Active in the docking of FBH1$_{PIP}$ and FBH1$_{APIM}$ residues of PCNA are colored red and blue, respectively. (b) Overlay of separately recorded ^{1}H-^{1}H TOCSY NMR spectra of FBH1$_{PIP}$ (orange), FBH1$_{APIM}$ (green), and PCNA (black). Only the region with amide-aliphatic proton correlation is shown. (c) Overlay of ^{1}H-^{1}H TOCSY spectra of PCNA with a 1:1:0 molar ratio of PCNA protomer:FBH1$_{PIP}$:FBH1$_{APIM}$ (blue) and of PCNA with a 1:1:70

molar ratio of PCNA protomer:$FBH1_{PIP}$:$FBH1_{APIM}$ (violet). Both spectra are plotted at the same contour level, and only positive contours are shown. Signals from free $FBH1_{PIP}$ are labeled with arbitrary numbers. Asterisks indicate spectral artefacts identified by an alternating pattern of negative and positive contours. (d) Plot of the intensity of observed $FBH1_{PIP}$ signals in the spectra shown in (c). The signals corresponding to peaks 3 and 6 (blue) are at the level of the noise. The error bars indicate twice the average intensity of the noise measured in a region devoid of signals. (e) AlphaFold structural model of the FBH1 UvrD domain from UniProt Q8NFZ0. The $FBH1_{APIM}$ amphipathic α-helix is colored green. The hydrophobic and positively charged residues are shown as sticks and labeled. (f) Overlay of the model shown in (e) with the crystal structure of the *Deinococcus radiodurans* UvrD (cyan) in complex with DNA (PDB ID: 4C2T).

Table 1.

Data collection and refinement statistics for PCNA in complex with three $FBH1_{PIP}$.

	PCNA:$FBH1_{PIP}$
Wavelength	
Resolution range	41.79 − 1.9 (1.968 − 1.9)
Space group	I 1 2 1
Unit cell	81.95 82.2096 118.558 90 91.2567 90
Total reflections	118405 (11431)
Unique reflections	60967 (6033)
Multiplicity	1.9 (1.9)
Completeness (%)	98.28 (97.78)
Mean I/sigma(I)	9.00 (1.99)
Wilson B-factor	25.28
R-merge	0.04254 (0.3397)
R-meas	0.06016 (0.4805)
R-pim	0.04254 (0.3397)
CC1/2	0.997 (0.567)
CC*	0.999 (0.851)
Reflections used in refinement	60946 (6027)
Reflections used for R-free	1997 (206)
R-work	0.2237 (0.3456)
R-free	0.2650 (0.3563)
CC(work)	0.948 (0.741)
CC(free)	0.918 (0.711)
Number of non-hydrogen atoms	6039
macromolecules	5783
solvent	256
Protein residues	744
RMS(bonds)	0.010
RMS(angles)	1.89
Ramachandran favored (%)	98.17
Ramachandran allowed (%)	1.83
Ramachandran outliers (%)	0.00
Rotamer outliers (%)	0.76
Clashscore	14.73
Average B-factor	37.24
macromolecules	37.03
solvent	41.98

Statistics for the highest-resolution shell are shown in parentheses.

KEY RESOURCES TABLE

REAGENT or RESOURCE	SOURCE	IDENTIFIER
Bacterial and Virus Strains		
Escherichia coli BL21-CodonPlus (De3) RIL	Agilent Technologies	N/A
Escherichia coli BL21 (DE3) Rosetta	Merk	70954
Chemicals, Peptides, and Recombinant Proteins		
Dithiothreitol	Melford	D11000
^{15}NH4Cl	Merck Sigma Aldrich	299251
IPTG	Neo Biotech	NB-45–00030
Deuterium Oxide	Merck Sigma Aldrich	756822
Lysozyme chloride form from chicken egg white	Merck Sigma-Aldrich	L-2879
Protease Inhibitors cOmplete ultra-tablets	Roche	11836170001
HisPur™ Ni-NTA beads	Thermo Fisher	88221
Sodium dihydrogen phosphate monohydrate	Merck	106346
Potassium Phosphate dibasic trihydrate	Merck Sigma	P9666
Celtone base powder ^{2}H, ^{13}C, ^{15}N	CIL	CGM-1030P-CDN-1
DSS	Deutero GmSH	D-56288
Thiamine hydrochloride	SIGMA	T1270
Biotin	Merck Sigma	B4639
Tricine	MELFORD	T2400
FBH1$_{PIP}$ peptide	Synpeptide	N/A
FBH1$_{APIM}$ peptide	Synpeptide	N/A
PreScission protease	Home expressed	N/A
Deposited Data		
Crystal structure of PCNA bound to FBH1$_{PIP}$ peptide	This study	PDB: 8F5Q
Recombinant DNA		
Plasmid: pET-47b	Addgene	71461–3
Modified pET28 with human PCNA gene	This study	Sanchez et al., 2007
Software and Algorithms		
iMosflm	Battye et al., 2011	https://www.mrc-lmb.cam.ac.uk/harry/imosflm
CCP4	Winn et al., 2011	https://www.ccp4.ac.uk/
Phenix	Adams et al., 2010	http://www.phenix-online.org/
Coot	Emsley et al., 2010	https://www2.mrc-lmb.cam.ac.uk/personal/pemsley/coot/
TopSpin 2.1 & TopSpin 3.5pl7	Bruker	https://www.bruker.com
CcpNmr Analysis	Vranken et al., 2005	https://www.ccpn.ac.uk
HADDOCK 2.4	Honorato et al., 2021	WeNMR/West-Life
PyMol	Schödinger	https://pymol.org/
MolProbity	Williams et al., 2018	http://molprobity.biochem.duke.edu/
Prism 9.1	GraphPad Software	https://www.graphpad.com